Journal of Microwaves, Optoelectronics and Electromagnetic Applications, Vol. 25, No. 3, e2026304414 Aug 2026
DOI: http://doi.org/10.1590/2179-10742026v25i3304414

Article

A Reconfigurable Complementary Frequency-Selective Surface with Single-, Dual-, and Attenuated-Passband Responses

Deisy F. Mamedes[1], Jens Bornemann[1], Alfredo Gomes Neto[2] Sérgio L. M. Sales-Filho[2]
[1]*Department of Electrical and Computer Engineering, University of Victoria, Victoria, BC, V8W 2Y2, Canada.*
j.bornemann@ieee.org, mamedes@ieee.org
[2]*Department of Electrical Engineering, Federal Institute of Paraiba, João Pessoa, PB, 58015-905, Brazil.*
alfredogomes@ieee.org, sergio.morais@academico.ifpb.edu.br

***Abstract*— This paper presents a reconfigurable frequency-selective surface (FSS) featuring switchable reflection and transmission characteristics based on a complementary-inspired four-arm star geometry. The design process begins with the independent analysis of a slot element and its complementary patch counterpart, which are subsequently integrated on a single-layer substrate. To enable electrical reconfigurability, the patch element is modified by adding a switching point to integrate a PIN diode along with bias lines for feeding. The electromagnetic response is evaluated across three diode operational states: off (reverse bias), on (forward bias), and threshold bias. For TE polarization, the structure exhibits a single-passband response near 3.75 GHz in the reverse-biased state and a dual-passband response near 2.1 GHz and 6.9 GHz in the forward-biased state, with a stopband between the two passbands. At the threshold voltage, the reconfigurable complementary FSS provides an attenuated-transmission state, enabling control of the transmitted signal level. These operating modes allow the same surface to switch between transmission, rejection, and attenuation, which is useful for adaptive filtering, interference mitigation, and signal-level control in intelligent 5G-Advanced communication network applications.**

***Index Terms*—** Frequency-selective surfaces, reconfigurable FSS, multi-band operation, duality theorem.

I. Introduction

Frequency-selective surfaces (FSSs) are two-dimensional arrays of periodic structures, typically formed by patch (conductive) or slot (aperture) elements etched on a dielectric substrate, which provide filtering properties for incident electromagnetic (EM) waves [1], [2]. The scattering behavior of FSSs is influenced by the geometry and periodicity of the elements, the thickness and electromagnetic characteristics of the dielectric substrate, as well as the polarization and angle of the incoming waves. These structures have found widespread applications, including as sub-reflectors of multiband antennas [3], [4], reconfigurable antennas [5], [6], polarization converters [7], [8], intelligent walls [9], [10], radar cross-section reduction [11], [12], and absorbers [13], [14].

In principle, FSSs are passive structures, meaning their electromagnetic characteristics remain unchanged after fabrication [15]. However, modern wireless communication systems demand adaptive performance to address challenges such as dynamic frequency allocation, interference mitigation, beam

Brazilian Microwave and Optoelectronics Society-SBMO
Brazilian Society of Electromagnetism-SBMag
received 10 Jan 2026; for review 31 Mar 2026; accepted 19 Jun 2026
Editor: Carlos E. Capovilla Associate Editor: Rafael A. Penchel
© 2026 SBMO/SBMag
CC BY
ISSN 2179-1074

control, and signal-level management in environments like 5G and 5G-Advanced networks. To meet these needs, reconfigurable FSSs (RFSSs) have been developed, allowing for dynamic modification of their frequency response of reflection and transmission spectra, even after fabrication. The two main methods of reconfiguring FSSs are electrical and mechanical. Electrical approaches incorporate active components, such as PIN diodes [16], [17], [18] or varactors [19], [20], [21], to manipulate the magnitudes and phases of the reflection and transmission coefficients by altering the element's geometry and effective size. Mechanical methods, in contrast, involve movable parts and physical modifications are applied to the panel like stretching [22], folding [23], [24] or rotating [25], [26] the FSS elements to tune the frequency response.

Despite these advances, existing RFSS designs often suffer from complexity, including multi-layer configurations, numerous active components per unit cell, intricate biasing networks requiring vias or additional lumped elements, and limited operational modes. For instance, electrically reconfigurable designs frequently employ multiple diodes or varactors with separate bias networks for each layer or frequency band, leading to higher fabrication costs and power requirements [16], [18], [21], [27]. Mechanical designs, while avoiding active electronics, necessitate driving apparatuses and may compromise angular stability or tuning range [23], [26].

To address these limitations, this work proposes a simple and easy-to-design FSS that achieves reconfigurable properties with reduced complexity. The structure uses a single dielectric substrate with metallizations on both sides, designed based on the duality theorem, and incorporates only one PIN diode per unit cell. The bias network is integrated within the array, connecting unit cells in parallel rows without vias or additional layers. The design starts from the independent analysis of a slot-type element and its complementary patch-type counterpart, which are then combined into a complementary-inspired structure. The patch element is modified by introducing a switching gap, a PIN diode, and bias lines, enabling electrical control of the frequency response.

A key innovation is the exploitation of three diode states—forward biased, reverse biased, and threshold voltage. In the forward-biased state, the reconfigurable complementary FSS (RCFSS) exhibits a dual-passband response, with transmission bands around 2 and 6.9 GHz and a stopband between them. In the reverse-biased state, the structure exhibits a single-passband response around 3.75 GHz. Thus, the same frequency region near 3.75 GHz can be switched between passband and stopband operation by changing the diode bias. The frequency bands selected in this work are intended for 5G NR Frequency Range 1 (FR1) applications rather than being limited only to conventional "sub-6 GHz" operation, including lower FR1 bands, C-band operation, and the upper FR1 range. The ability to switch among these bands is useful in adaptive scenarios, where a surface may be required to transmit selected channels, reject interfering signals, or attenuate strong incident fields. In the threshold region, the diode introduces an intermediate resistive state, producing an attenuated-passband response. This controlled attenuation can be useful in 5G applications to reduce excessive received power, avoid front-end saturation, mitigate interference, or provide an automatic-gain-control-like spatial filtering function.

Compared to prior works, such as the three-mode design in [18] which requires eight diodes and multi-layer biasing for single/dual/no-passband operation, or the miniaturized varactor-based design in [27] with 12 varactors and superior angular stability (60°) but higher complexity, the proposed RFSS offers advantages in simplicity, low power (2 V DC), miniaturization (unit cell size of $0.11\lambda \times 0.11\lambda$), and angular stability up to 50° (detailed comparisons are provided in Table I in Section IV-C). These

Brazilian Microwave and Optoelectronics Society-SBMO received 10 Jan 2026; for review 31 Mar 2026; accepted 19 Jun 2026
Brazilian Society of Electromagnetism-SBMag Editor: Carlos E. Capovilla Associate Editor: Rafael A. Penchel
© 2026 SBMO/SBMag
ISSN 2179-1074

features make it particularly suitable for 5G applications as a reconfigurable intelligent surface, where its frequency bands align with sub-6 GHz allocations, and its mode-switching capability supports adaptive beam steering, interference control, and energy-efficient operation in dynamic environments.

The primary objective of this paper is to introduce a novel RFSS design that advances the state of the art by offering multi-mode reconfigurability with minimal complexity. This design demonstrates superior performance in terms of fabrication simplicity, low-voltage operation, and applicability to 5G systems. The remainder of the paper is organized as follows: Section II presents the design and analysis of the single-layer FSS, including simulated results; Section III describes the design of the proposed reconfigurable complementary FSS; Section IV provides performance validation through comparisons of simulated and measured results, along with an assessment against other published works; and Section V concludes the paper.

II. Single-layer FSS Analysis and Design

This section presents the design and analysis of a unit-cell FSS based on the four-arm star geometry with a slot-type element and its complementary one (patch type), individually, on single-layer substrate. The patch-type element is modified by inserting a gap in the center of the unit cell (to act as a switching point) to provide reconfiguration functionality. Initially, the single-metallic layer structure is analyzed considering the passive configuration, i.e., the ideal structure. Then, a PIN diode is used as an active component to reconfigure the FSS transmission characteristic, named practical FSS. The numerical characterizations of all structures are obtained through the commercial software package CST Microwave Studio. The dielectric substrate considered in the simulation has ϵ_r = 4.4, thickness of 1.0 mm, and loss tangent of 0.025.

A. Four-arm star slot-type FSS

The first structure is the slot type. In this case the outside of the element has metallic filling, which provides transmission of the incident EM waves at the desired frequency. Fig. 1a illustrates the unit cell with this element, including its parameters. The following steps are performed to achieve this configuration; the unit cell dimension is defined as p_s, and then a rectangular patch is designed as a_s, where the arms are shaped. From the edges, lines cross the rectangular patch with b_s are drawn, and the star geometry is achieved with pointed arms. A small square slot of width s_s is etched out at the center to connect all the slotted arms which completes the slotted four-arm star unit cell.

The design process to estimate the first resonant frequency of the four-arm star slot-type FSS can be carried out using the following steps:

$$f_{\text{slot}} = \frac{c}{2a_s\sqrt{\epsilon_{reff}}} \tag{1}$$

where a_s is the size of the four-arm star.

Reference [28] presents an interpolating formula that fits the variation of the effective permittivity

$$\epsilon_{reff} = \epsilon_r + (\epsilon_r - 1)\left[\frac{-1}{e^{\frac{10h}{p_s}N}}\right] \tag{2}$$

which considers the dielectric permittivity and thickness of the substrate h, periodicity p_s, and the exponential factor, *N*, of the unit cell filling. For the geometry proposed, the value of *N* is 3.8.

Brazilian Microwave and Optoelectronics Society-SBMO received 10 Jan 2026; for review 31 Mar 2026; accepted 19 Jun 2026
Brazilian Society of Electromagnetism-SBMag Editor: Carlos E. Capovilla Associate Editor: Rafael A. Penchel
© 2026 SBMO/SBMag
ISSN 2179-1074

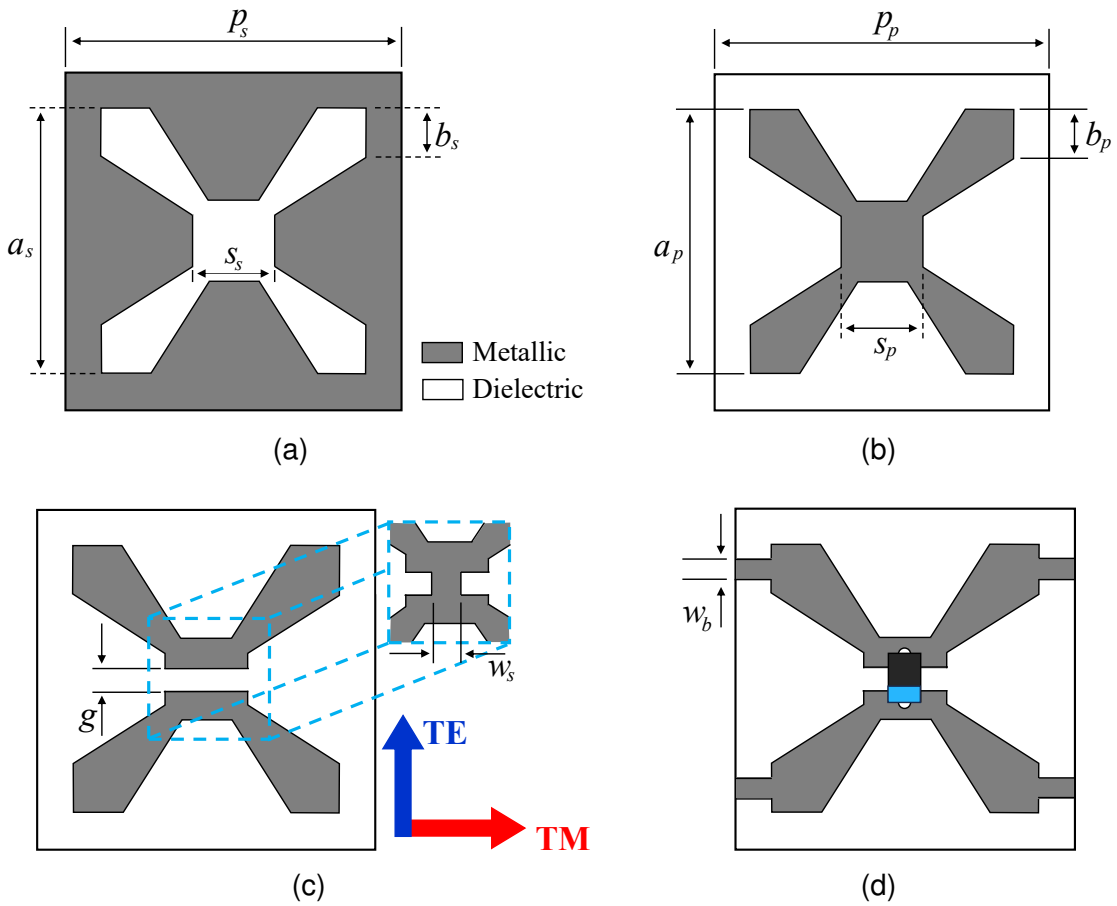


Fig. 1. Geometry and parameters of single-layer (a) slot-type, (b) ideal symmetric patch-type, (c) ideal asymmetric patch-type, and (d) practical patch-type, with bias lines and diode, FSSs.

Based on the equations above, the dimensions are p_s = 16 mm, a_s = 15 mm, b_s = 3 mm and s_s = 3 mm. The frequency response of this structure is shown in Fig. 2a,b (blue curves), with resonant frequency at 4.8 GHz. Note that this structure is symmetrical, leading to the same frequency response for the TE and TM polarizations at normal incidence.

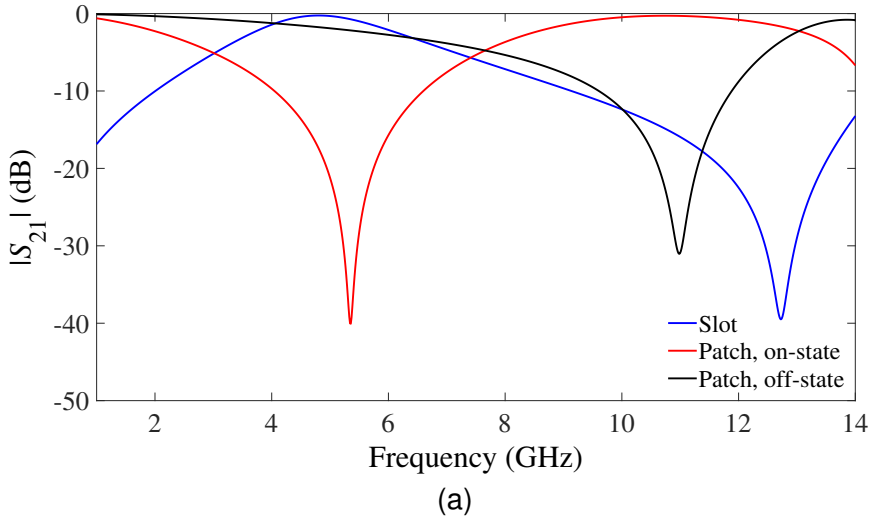
B. Four-arm star patch-type FSS

The design procedure of the symmetrical four-arm star patch type is similar to the slot one, except that in this case the outside of the element is detached from the metallic surface. Fig. 1b shows the symmetric patch unit cell with its parameters. The patch-type structure is designed as the complement of the slot one, i.e., they have the same dimensions ($p_p = p_s$, $a_p = a_s$, $b_p = b_s$ and $s_p = s_s$). This structure behaves as a stop-band filter with resonant frequency at 5.35 GHz (Fig. 2, red curves). Although the duality theorem states that the designs of complementary elements provide opposite passband and stopband in the same frequency, from Fig. 2a,b we can see that the resonant frequency for the symmetric slot and patch elements are not the same with a difference of 10%. This is due to the fact that the element arrays are built on a substrate slab, i.e., they are not free-standing, shifting their resonant frequency. As expected for the symmetrical structure, the TE and TM polarizations present the same characteristics.

To form different reconfiguration states, a gap g is added to the original geometry as a switching point. The unit cell of the patch-type FSS with the new parameter added is illustrated in Fig. 1c. The

Brazilian Microwave and Optoelectronics Society-SBMO
Brazilian Society of Electromagnetism-SBMag
received 10 Jan 2026; for review 31 Mar 2026; accepted 19 Jun 2026
Editor: Carlos E. Capovilla Associate Editor: Rafael A. Penchel
© 2026 SBMO/SBMag
ISSN 2179-1074

gap provides an asymmetric element, where the upper and lower arms are physically disconnected. In this scenario, the horizontal electric field sees that the arms are electrically connected for the TM polarization. For the TE polarization, as shown in Fig. 1c, the vertical electric field is maximum in the center of the unit cell, seeing the perturbation. In this case, the arms are physically and electrically disconnected, and the gap is seen now as an additional capacitance to the circuit, leading to different transmission coefficients for each polarization. The asymmetry of the element is provided by a gap of 0.8 mm, characterized as patch-type in the off-state. The gap width is designed based on the available diode size. Fig. 2 shows the results of the asymmetric geometry. As predicted, the resonant frequency is moved in the TE polarization to 10.98 GHz (Fig. 2a, black curve), while for the TM polarization it is unaltered, presenting the same response as for the symmetric element (Fig. 2b, black curve).



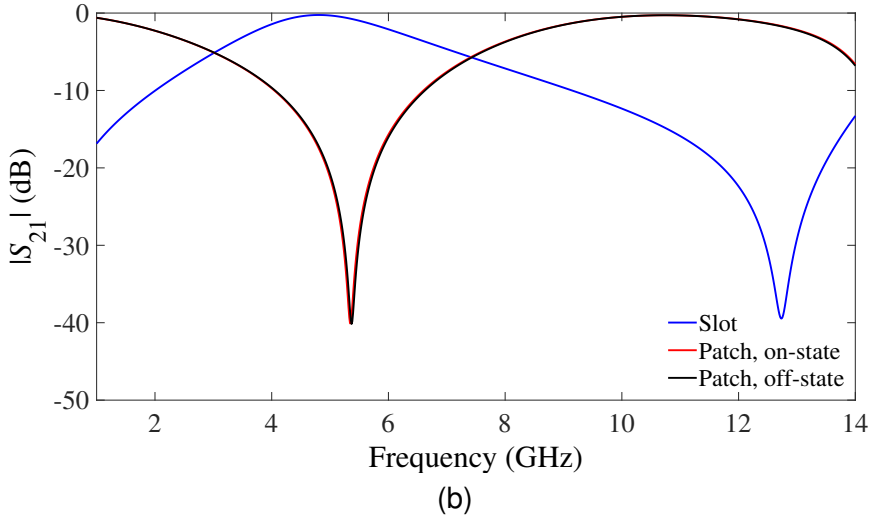


Fig. 2. Numerical results for (a) TE and (b) TM polarization of slot-type and patch-type, in the on- and off-state without bias lines, ideal elements FSSs.

Analyses of the proposed structure in the ideal state conditions are performed to estimate the frequency response of the practical FSS. The first ideal case consists of the unit cell with all the arms connected by a strip line with width w_s (Fig. 1c), providing a similar characteristic as if the PIN

Brazilian Microwave and Optoelectronics Society-SBMO
Brazilian Society of Electromagnetism-SBMag
received 10 Jan 2026; for review 31 Mar 2026; accepted 19 Jun 2026
Editor: Carlos E. Capovilla Associate Editor: Rafael A. Penchel
© 2026 SBMO/SBMag
ISSN 2179-1074

diode were forward biased. In the second condition, the upper and lower arms are physically separated by the gap g, acting as if the PIN diode was not biased. The connection of the arms can be restored by the width w_s with different sizes. To achieve the perfect complementary (or symmetric) structure, w_s must be equal to s_p, which is the patch-type in the on-state.

As mentioned above, the ideal structures emulate the characteristic of the practical one. In order to more accurate predict the frequency response of the practical patch-type FSS when in on-state, an evaluation of the strip line's size is performed, considering w_s = 0.1 mm, 1.0 mm and 3.0 mm. The electrical model of the PIN diode when forward biased is an inductor in series with a resistor. The conducting strip provides an inductance characteristic to the FSS when the electric field is parallel to it. As w_s decreases, the transmission minimum is moved to lower frequency, getting closer to the actual response if a PIN diode was used. Fig. 3a presents the simulated results for this analysis. The resonant frequencies for w_s = 0.1 mm, 1.0 mm and 3.0 mm are 4.42 GHz (blue curve), 4.9 GHz (red curve) and 5.35 GHz (black curve), respectively, for TE polarization. When the electric field is perpendicular

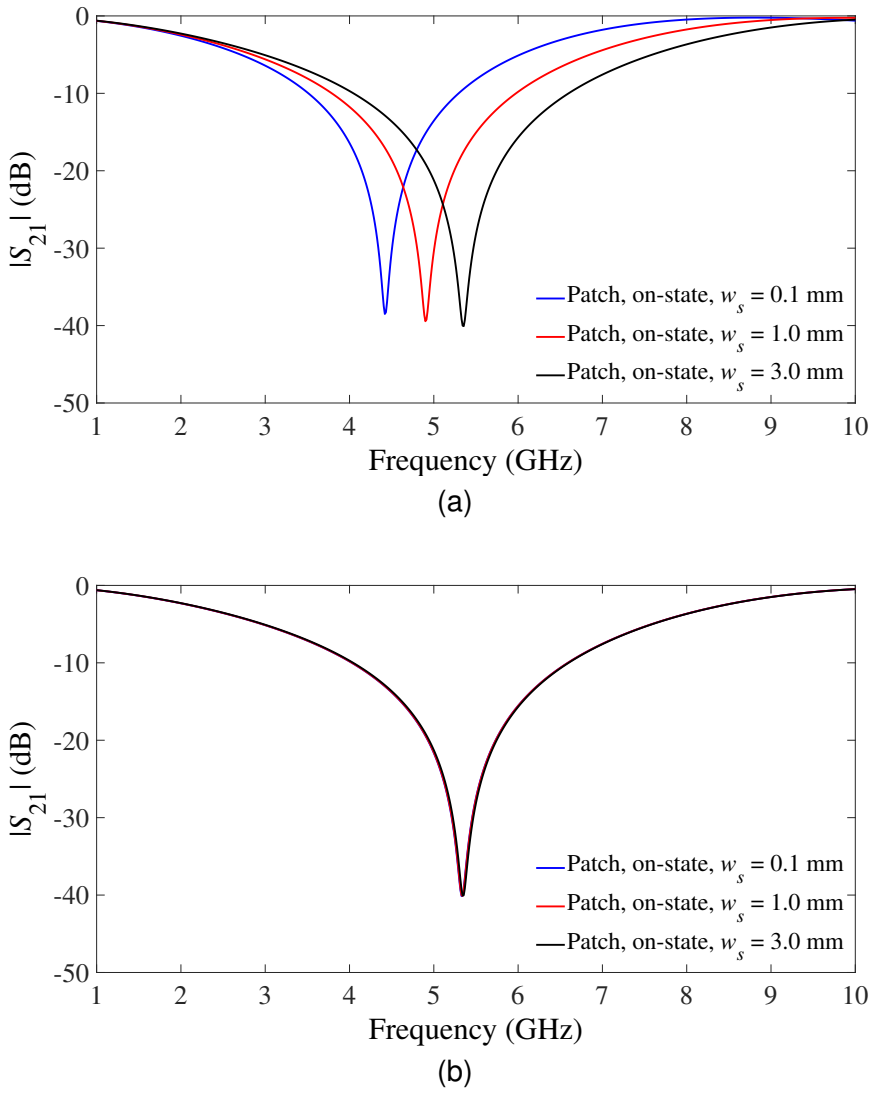
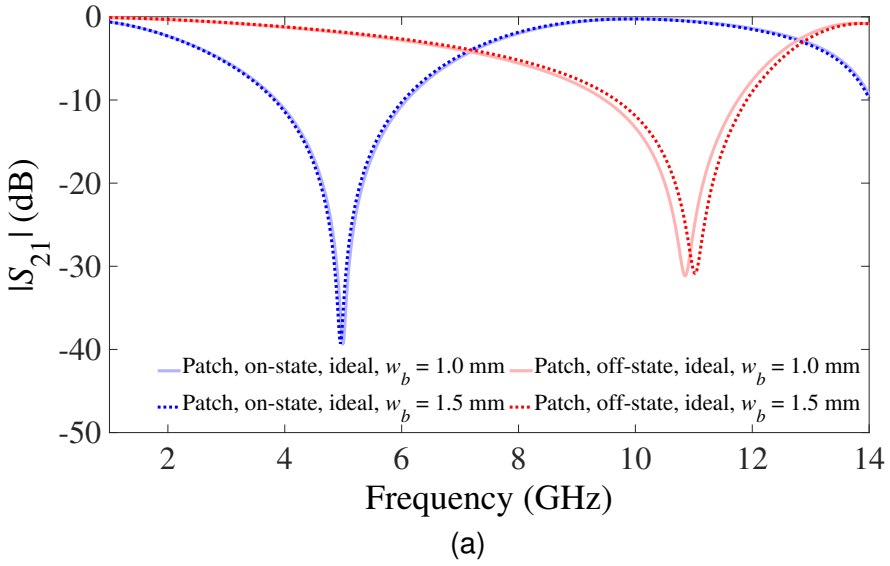


Fig. 3. Numerical results for (a) TE and (b) TM polarization of patch-type in the on-state, without bias lines, ideal elements FSSs as a function of strip size w_s.

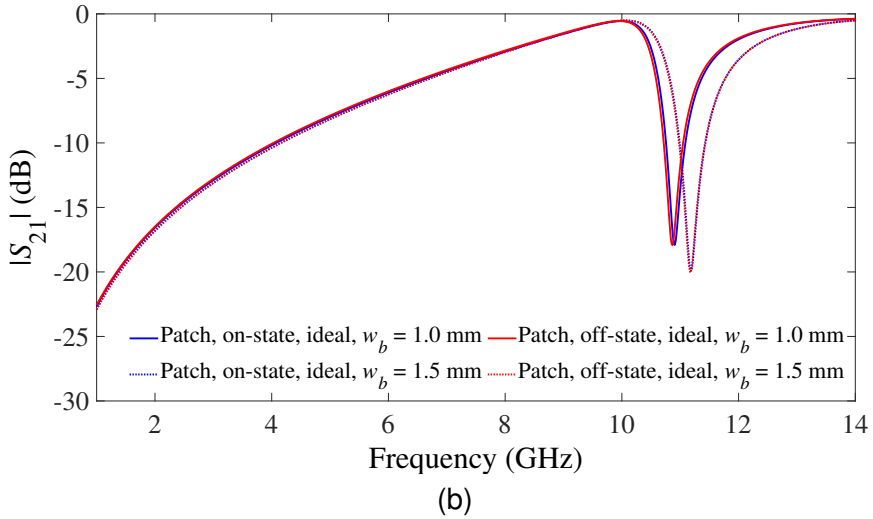
Brazilian Microwave and Optoelectronics Society-SBMO
Brazilian Society of Electromagnetism-SBMag
received 10 Jan 2026; for review 31 Mar 2026; accepted 19 Jun 2026
Editor: Carlos E. Capovilla Associate Editor: Rafael A. Penchel
© 2026 SBMO/SBMag
ISSN 2179-1074

to the FSS, it is practically null in the center of the unit cell, which makes it not being affected by the different w_s sizes, with resonant frequency at 5.34 GHz for all cases (Fig. 3b). Due to limitation in the manufacture process, the width chosen for w_s for the ideal on-state condition is set to 1.0 mm.

The passive model provides a good understanding of the reconfigurability of the element, but in practice the electronic model uses an active component (e.g. PIN diode). The biasing circuit is another key element in the design of the RFSS, and it is difficult to incorporate the active component along with the FSS' element. It is found in the literature that the feeding plane can be performed using an extra layer [29], and vias can be used to connect the element's layer to the biasing network [30]. Furthermore, some of these biasing systems have the diodes connected in series [31], [32], requiring high voltage level power supplies. However, in this work, the entire diode bias network is placed in the same plane as the FSS' element by adding bias lines horizontally with width w_b in the edges of each arm as shown in Fig. 1d. The size of w_b almost has no effect on the frequency response of the FSS in



(a)



(b)

Fig. 4. Numerical results for (a) TE and (b) TM polarization of patch-type in the on- and off-state ideal elements FSSs as a function of bias lines size w_b.

Brazilian Microwave and Optoelectronics Society-SBMO
Brazilian Society of Electromagnetism-SBMag
received 10 Jan 2026; for review 31 Mar 2026; accepted 19 Jun 2026
Editor: Carlos E. Capovilla Associate Editor: Rafael A. Penchel
© 2026 SBMO/SBMag
ISSN 2179-1074

both states for the TE polarization, where the resonant frequency is determined by the size of the arms (Fig. 4a). However, in the TM polarization, the FSS frequency response changes completely, showing to be dependent on w_b, creating a transmission maximum that gradually inclines and then declines steeply to the transmission minimum that is up-shifted (Fig. 4b). By incorporating a PIN diode with the bias lines into the unit cell, the four-arm star patch-type is split, which shifts the resonant frequency in one polarization, because the structure becomes polarization dependent, due to its asymmetry in the x- and y-directions. Switching the PIN diode on or off changes the effective inductance and capacitance of the element.

To further understand the physical mechanism responsible for the polarization-dependent response, Fig. 5 shows the electric-field and surface-current distributions on the patch-type FSS at their respective resonance frequencies. For TE polarization in the on-state, the electric field is mainly confined along the edges of the arms, whereas the surface current is strongly concentrated around the switching point, where the PIN diode is located, as shown in Fig. 5a. Therefore, the diode directly affects the main current path and changes the effective electrical connection between the upper and lower arms. In the off-state under TE polarization, the upper and lower arms are disconnected. As a result, a strong electric field is established across the switching gap, while the surface current is restricted to the arm sections between the arm edges and the switching point, as illustrated in Fig. 5b. This disconnected configuration introduces a different effective capacitance and inductance in the unit cell, which shifts the resonance frequency to a higher value. Consequently, the TE-polarized transmission response changes significantly between the on- and off-states. For TM polarization, the on-state and off-state distributions, shown in Figs. 5c and 5d, are very similar. In this case, the electric field is nearly null at the switching point and is mainly concentrated along the arm segments, while the surface current flows predominantly through the bias-line region. Therefore, the PIN diode is weakly excited for TM incidence, and changing its bias state from forward to reverse bias produces only a negligible modification of the effective capacitance and inductance of the unit cell. This explains why the TM-polarized transmission response remains

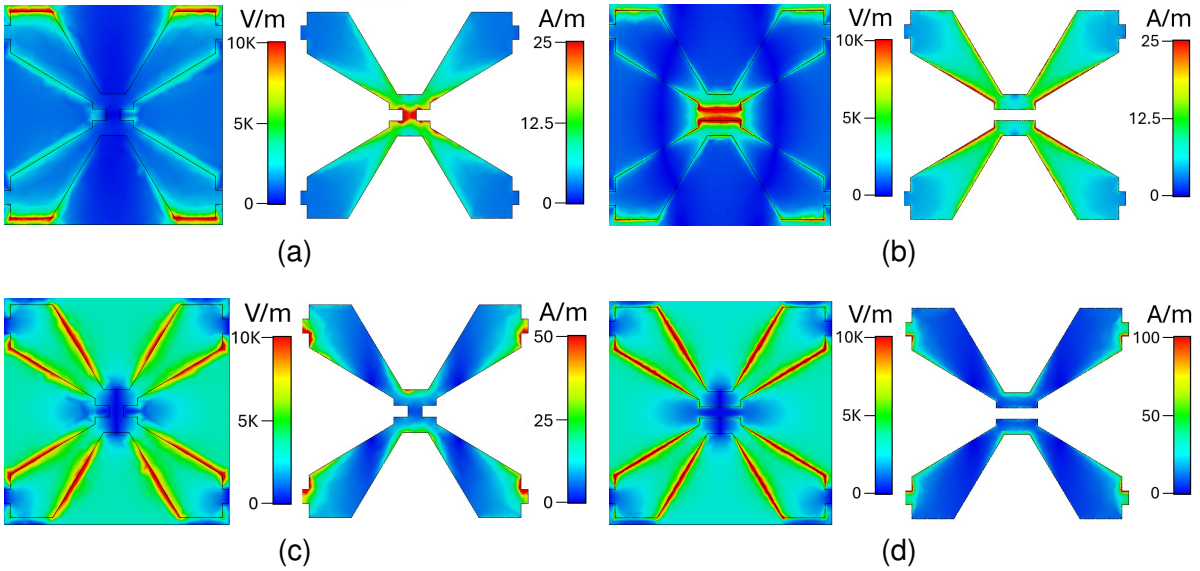


Fig. 5. Distributions of electric field (left) and surface current (right) on the patch-type FSS under normal incidence for TE polarization in the (a) on-state and (b) off-state, and for TM polarization in the (c) on-state and (d) off-state.

Brazilian Microwave and Optoelectronics Society-SBMO
Brazilian Society of Electromagnetism-SBMag
received 10 Jan 2026; for review 31 Mar 2026; accepted 19 Jun 2026
Editor: Carlos E. Capovilla Associate Editor: Rafael A. Penchel
© 2026 SBMO/SBMag
ISSN 2179-1074

almost unchanged between the on- and off-states, whereas the TE-polarized response exhibits a clear frequency shift.

The ideal and practical structures with the patch-type element in its final configuration were characterized numerically and the computed magnitude of transmission coefficients is shown in Fig. 6. The bias lines have w_b = 1 mm. The Skyworks SMP1340-079LF PIN diode was selected because its RF switching characteristics are suitable for the operating frequency range of the proposed structure; in the simulations, the manufacturer-provided Touchstone files were used to accurately model the diode in both on- and off-state [33]. When in the on-state, all arms are connected and the resonant frequencies for the ideal and practical structures are 4.99 GHz and 4.79 GHz (Fig. 6a), respectively, for the TE polarization, with maximum difference of 4%. It can be seen in Fig. 6a that by loading the off-state, the stopband of the ideal with reference to practical FSSs is up-shifted significantly due to the added capacitance between the gap in the center of the unit cell. The off-state FSS resonates at 10.85 GHz and 8.36 GHz for the ideal and practical cases, respectively. When the PIN diode is reversed biased,

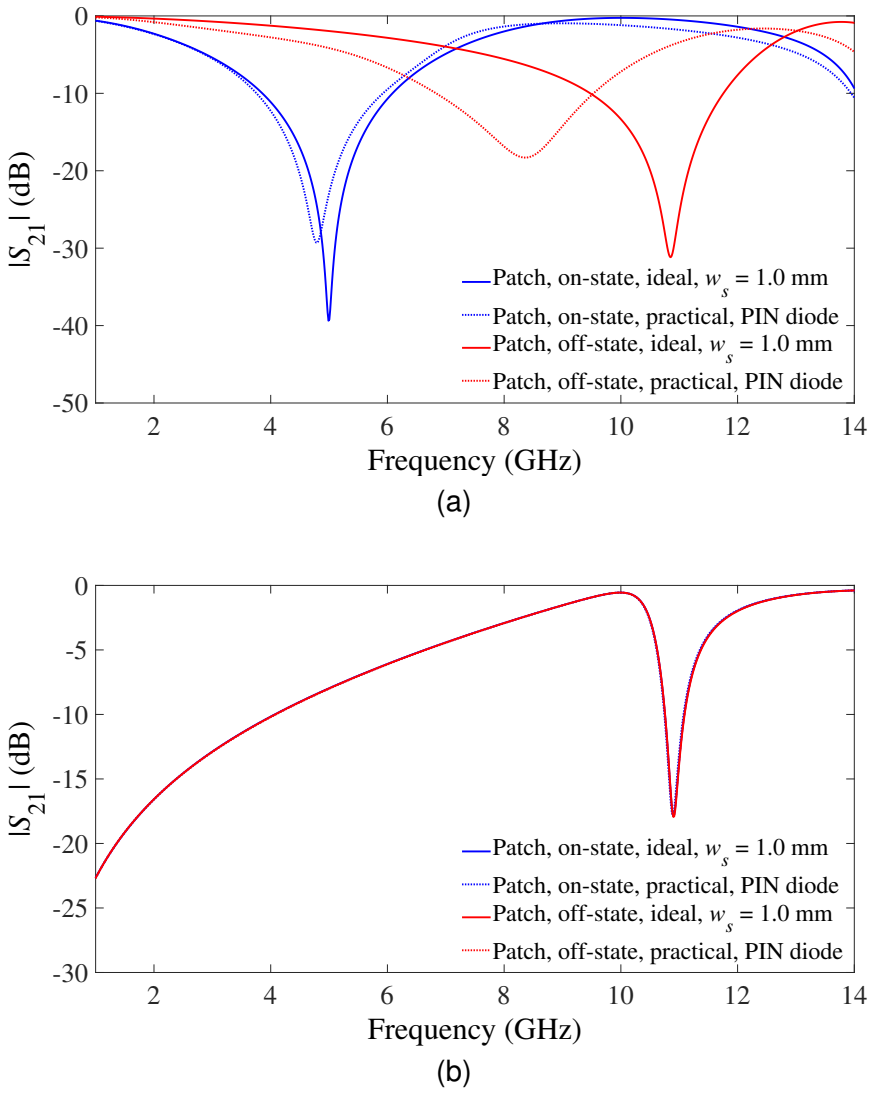


Fig. 6. Comparison of frequency response of the ideal and practical patch-type elements FSSs with bias lines in the on- and off-state for (a) TE and (b) TM polarization.

Brazilian Microwave and Optoelectronics Society-SBMO
Brazilian Society of Electromagnetism-SBMag
received 10 Jan 2026; for review 31 Mar 2026; accepted 19 Jun 2026
Editor: Carlos E. Capovilla Associate Editor: Rafael A. Penchel
© 2026 SBMO/SBMag
ISSN 2179-1074

its circuit comprises of a capacitor with a large shunt resistor. Reference [33] suggests that the PIN diode in this condition (at V = 0 V) offers a capacitance of 0.24 pF. Note that the resonance difference of the ideal and practical FSS is associated with the fact that the gap g does not emulate the same capacitance as the PIN diode. Although this difference could be compensated by reducing the gap size, g = 0.8 mm was maintained because it was the smallest gap that could be reliably implemented with the available fabrication process. Fig. 6b shows the results in the TM polarization; it is observed that the bias lines affect the transmission responses due to its inductance when compared to those in Fig. 3b. As explained above, for the TM polarization, the on/off state present the same resonant frequency at 10.9 GHz, because the electric field vanishes in the diode area.

III. Reconfigurable Complementary FSS Design

This section describes the design procedure of a complementary-based FSS with reconfigurability features based on Babinet's principle for electromagnetic fields [34], [35], [36], [37]. The reconfigurable complementary FSS (RCFSS) proposed in this paper combines the slot-type element and asymmetric patch-type element with bias lines, both topologies presented in the previous section. The slot-type FSS behaves primarily as a bandpass spatial filter, allowing transmission near its resonant frequency, whereas the patch-type FSS behaves primarily as a bandstop spatial filter, reflecting the incident wave near resonance. Therefore, the two structures provide complementary filtering responses. In an ideal free-standing complementary pair, Babinet's principle predicts opposite transmission and reflection characteristics at the same frequency.

The complementary structure is achieved by designing the patch and slot elements using identical geometry shape and dimensions, and these elements are spaced by a substrate. We do not truly follow this approach because the shape of the patch element is disturbed by the gap inserted in the center of the unit cell and bias lines in the edges of the arms. For this reason, the proposed structure can be understood as a quasi-complementary or complementary-inspired FSS. Fig. 7 illustrates the three-dimensional unit-cell topology of the proposed RCFSS. The medium used to separate the elements is a dielectric substrate with thickness h and dielectric constant ϵ_r. The top layer of the substrate is formed

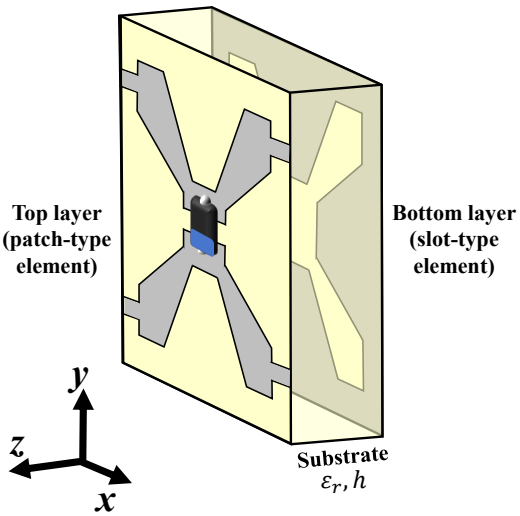


Fig. 7. RCFSS structuring.

Brazilian Microwave and Optoelectronics Society-SBMO
Brazilian Society of Electromagnetism-SBMag
received 10 Jan 2026; for review 31 Mar 2026; accepted 19 Jun 2026
Editor: Carlos E. Capovilla Associate Editor: Rafael A. Penchel
© 2026 SBMO/SBMag
ISSN 2179-1074

by the patch element, while the bottom layer carries the slot one.

The combination of the slot and patch layers introduces electromagnetic coupling between the bandpass and bandstop responses. This coupling miniaturizes the overall frequency response when compared with the isolated single-layer elements. Therefore, although the isolated off-state patch-type FSS presents a resonance above 10 GHz, as shown in the single-layer analysis, the coupled RCFSS shifts the useful operating responses to lower frequencies. This explains why the single-layer structures were analyzed over a wider frequency range, while the final RCFSS operates in the frequency range of interest for 5G NR FR1 applications.

The reconfigurability of the proposed RCFSS is controlled by the PIN diode inserted in the patch-type element. When the diode is forward biased, the upper and lower patch arms are electrically connected, increasing the coupling between the patch and slot layers. Under this condition, the RCFSS is expected to provide a dual-passband response, with a stopband located between the two transmission bands. When the diode is reverse biased, the patch arms are effectively separated by the diode capacitance, and the coupling between the two layers is modified. In this state, the structure exhibits a single-passband response, mainly associated with the slot-type element and the coupled complementary configuration. At the diode threshold region, the equivalent diode resistance is neither sufficiently low to fully connect the patch arms nor sufficiently high to fully isolate them. As a result, the structure provides an intermediate attenuated-transmission state instead of a conventional fully transmissive or reflective response.

The polarization behavior is also determined by the position of the switching gap and by the orientation of the bias lines. For TE polarization, the electric field is strong across the central gap of the patch element. Consequently, the diode state significantly changes the effective capacitance and inductance of the unit cell, producing a clear reconfiguration of the transmission response. For TM polarization, the electric field is nearly null at the switching point, as discussed in Section II. Therefore, the diode state has a weaker influence on the frequency response. Nevertheless, the horizontal bias lines still perturb the current path and contribute to the higher-frequency transmission features observed for this polarization. This explains why the TE response exhibits stronger switching between single-passband, dual-passband, and attenuated-passband states, while the TM response is less sensitive to the diode bias condition.

In this work, the RCFSS was designed with the same dimensions used for the individual FSSs presented in Section II. Fig. 8 illustrates the equivalent circuit for the proposed RFSS, which combines the equivalent circuits of the patch element (series LC) with a PIN diode and slot element (parallel LC). Note that an impedance Z_d is added to account for the mutual coupling between the metallic layers.

IV. Performance Validation

Experimental characterizations of the proposed reconfigurable CFSS-based configuration were performed to validate the numerical results. All prototypes were manufactured on a single-layer low-cost FR-4 fiber-glass dielectric substrate and metallization are on both sides, with ϵ_r = 4.4, thickness of 1.0 mm, and tanδ $= 0.025$. Three FSSs were fabricated to examine the scattering properties, being two passive CFSSs and one active CFSS. The fabricated prototypes are presented in Fig. 9 with the close-up view of the unit cells. The fabricated CFSSs have 12 $\times$ 12 elements and overall dimensions of 19.2 cm $\times$ 19.2 cm. Fig. 9a shows the array formed by slot elements found in the bottom layer of

Brazilian Microwave and Optoelectronics Society-SBMO received 10 Jan 2026; for review 31 Mar 2026; accepted 19 Jun 2026
Brazilian Society of Electromagnetism-SBMag Editor: Carlos E. Capovilla Associate Editor: Rafael A. Penchel
© 2026 SBMO/SBMag
ISSN 2179-1074

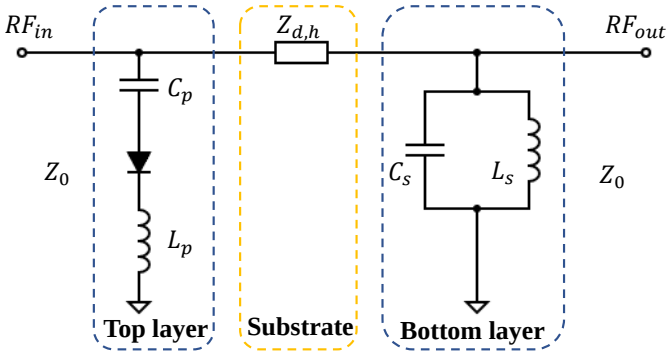


Fig. 8. RFSS equivalent circuit.

all structures. Fig. 9b and Fig. 9c show the top view of the passive CFSS in the on- and off-states, respectively. The diode-mounted RCFSS is shown in Fig. 9d with a total of 144 diodes soldered on it. The surface-mountable Skyworks SMP1340-079LF PIN diodes in plastic package, with parasitic inductance of 0.7 nH, are used. The package length and width are 1.1 mm and 0.7 mm, respectively. When forward biased, these diodes offer low resistance with typical value of 0.85 Ω at 10 mA and 0.85 V. When reverse biased, they can reach a capacitance as low as 0.21 pF at 5 V [33].

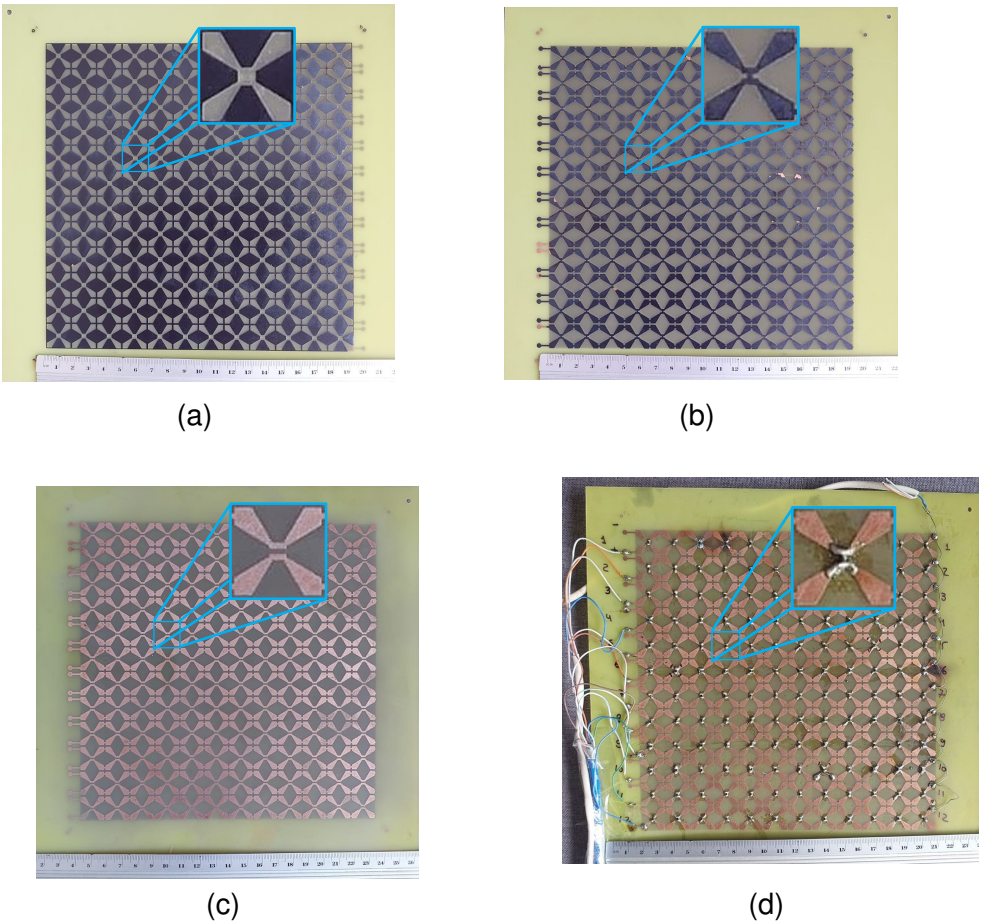


Fig. 9. Fabricated complementary structures: (a) slot elements present in all structures (bottom view), (b) ideal CFSS on-state (top view), (c) ideal CFSS off-state (top view), and (d) RCFSS with diodes (top view).

Brazilian Microwave and Optoelectronics Society-SBMO
Brazilian Society of Electromagnetism-SBMag
received 10 Jan 2026; for review 31 Mar 2026; accepted 19 Jun 2026
Editor: Carlos E. Capovilla Associate Editor: Rafael A. Penchel
© 2026 SBMO/SBMag
ISSN 2179-1074

The bias lines connect the diodes in parallel, allowing each FSS row to be independently controlled, while applying low voltage levels. A resistor of 230 Ω is added in series to each FSS' row to limit the current flowing through the diodes, as illustrated in Fig. 10. The biasing circuitry is formed by using single-core wires as shown in Fig. 9d, connected to auxiliary strip lines of 8 mm. The biasing network indicates that there are 12 diodes connected in parallel per row, and a total of 12 rows. Under the forward-bias condition, the complete RCFSS prototype draws a total current of 53 mA at 2 V DC, corresponding to a total power consumption of only 106 mW.

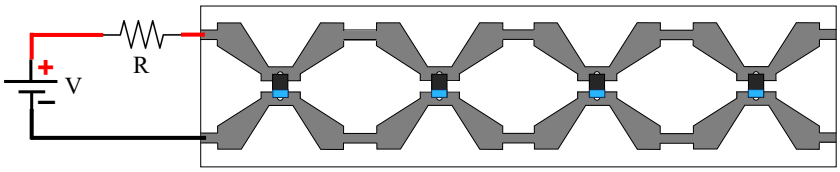


Fig. 10. Biasing schematic per RFSS' row.

Measurements were carried out using an Agilent E5071C ENA two-port vector network analyzer (frequency range from 300 kHz to 20 GHz), two SAS-571 double ridge horn antennas (frequency range from 700 MHz to 18 GHz, and linearly polarized), an Agilent E3631A DC power supply (triple output: 0 – ±25 V, 0 – 1A; 0 – 6 V, 0 – 5A; 80 W) and a measurement window. The two horn antennas were placed facing each other at a fixed position, with a distance of 150 cm to ensure that the transmitter and receiver antennas are in the far-field regions (Fig. 11). The measured transmission coefficients shown in Figs. 12 – 16 are computed by subtracting the transmission spectra of each polarization without the devices under test. The incidence of the wave to the FSSs is considered to be at normal ($\theta = 0°$) and oblique ($\theta =$ up to $50°$). The characterizations were performed sweeping θ in steps of $10°$, but we will only exhibit the results for $\theta = 0°$, $20°$ and $50°$, because the measured and simulated results agreed for all angles.

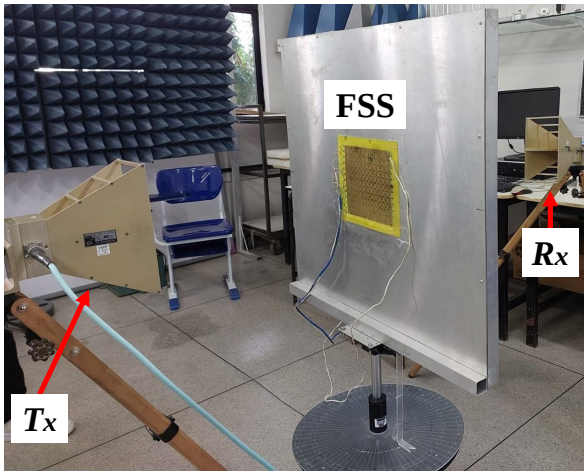


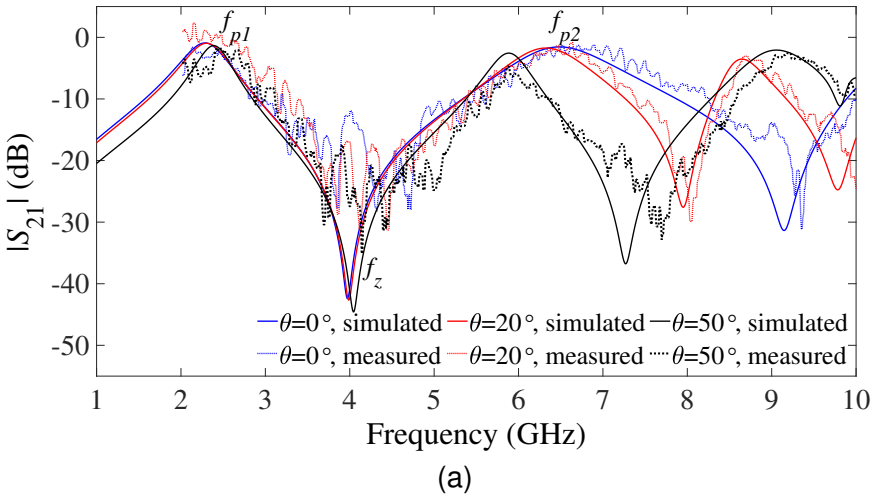
Fig. 11. Measurement setup.

A. *Passive CFSS Results*

When the elements of the proposed FSS are assembled in quasi-complement of one another, i.e., the patch element is in on-state, a dual-band response is expected due to their coupling. The numerical

Brazilian Microwave and Optoelectronics Society-SBMO
Brazilian Society of Electromagnetism-SBMag
received 10 Jan 2026; for review 31 Mar 2026; accepted 19 Jun 2026
Editor: Carlos E. Capovilla Associate Editor: Rafael A. Penchel
© 2026 SBMO/SBMag
ISSN 2179-1074

and measured results of the transmission coefficient for the ideal CFSS when it is in the on-state are presented in Fig. 12. The ideal CFSS in the on-state has a strip line of w_s = 1.0 mm to emulate the forward-biased PIN diode. The numerical characterization shows two transmission maxima (f_{p1} and f_{p2}) at 2.29 GHz and 6.48 GHz, and a transmission minimum (f_z) at 3.97 GHz for the TE polarization at normal incidence (Fig. 12a). The experimental characterization confirmed the result from simulation with f_{p1} = 2.14 GHz, f_{p2} = 6.53 GHz and f_z = 3.83 GHz. It is observed that for oblique incidence, the first transmission maximum and transmission minimum remain almost the same, but the second transmission maximum down-shifts as θ increases. As explained in Section II-B, the bias lines create a transmission maximum at a higher frequency for the patch element in the TM polarization. When this element is combined with the slot one, two transmission maxima appear to be closely spaced as illustrated in Fig. 12b. The first transmission maximum is found at 5.68 GHz (simulated) and 5.84 GHz (measured), while the second transmission maximum is at 7.81 GHz (simulated) and 8.06 GHz (measured), with a transmission minimum between them at 6.89 GHz (simulated) and 7.02 GHz (measured) at normal incidence, with frequency separation ratio of 1.37. For oblique incidence, the first



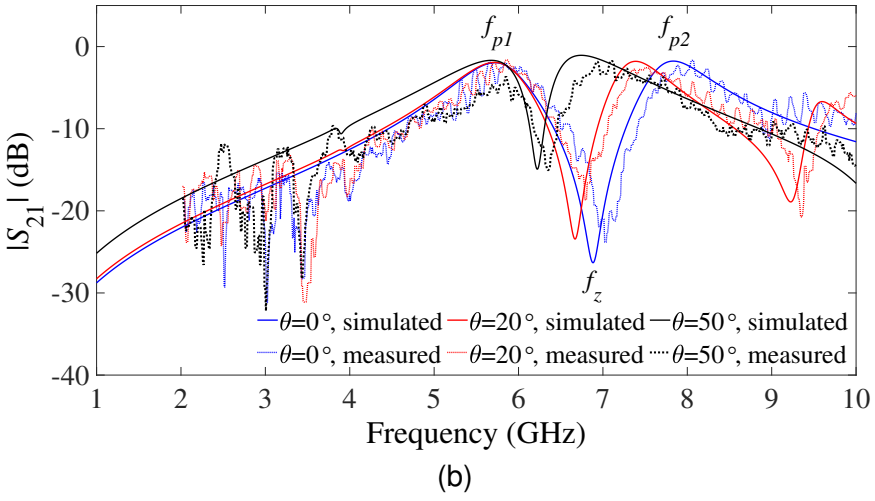


Fig. 12. Simulated and measured results for (a) TE and (b) TM polarization of ideal RCFSS in the on-state.

Brazilian Microwave and Optoelectronics Society-SBMO
Brazilian Society of Electromagnetism-SBMag
received 10 Jan 2026; for review 31 Mar 2026; accepted 19 Jun 2026
Editor: Carlos E. Capovilla Associate Editor: Rafael A. Penchel
© 2026 SBMO/SBMag
CC BY
ISSN 2179-1074

transmission maximum remains the same, while the transmission minimum and second transmission maximum move closer to the first one when θ increases, with frequency separation ratio of 1.19 for $\theta = 50°$.

The ideal case for the CFSS when the patch element is in the off-state was analyzed numerically and experimentally, and its transmission spectra is shown in Fig. 13. In this condition, the gap g emulates the reverse-biased PIN diode, and the capacitance offered by the gap shifts the resonant frequency of the patch element, as shown in Section II-B, for the TE polarization. The elements are decoupled for this state and only one passband is seen for this frequency range, which correspond to the response characteristic provided by the slot element. At $\theta = 0°$, the simulated and measured transmission maximum (f_p) is at 4.31 GHz and 3.62 GHz, respectively (Fig. 13a). The angular incidence was analyzed, and the results showed that the structure is stable up to $\theta = 50°$. The numerical and measured results for the TM polarization over different incident angles are presented in Fig. 13b. In this case, the response is very similar to that obtained for the TM polarization of the on-state passive CFSS shown in Fig. 12b, since the electric field is almost null at the center of the unit cell and, therefore, the gap has little influence on the transmission characteristics.

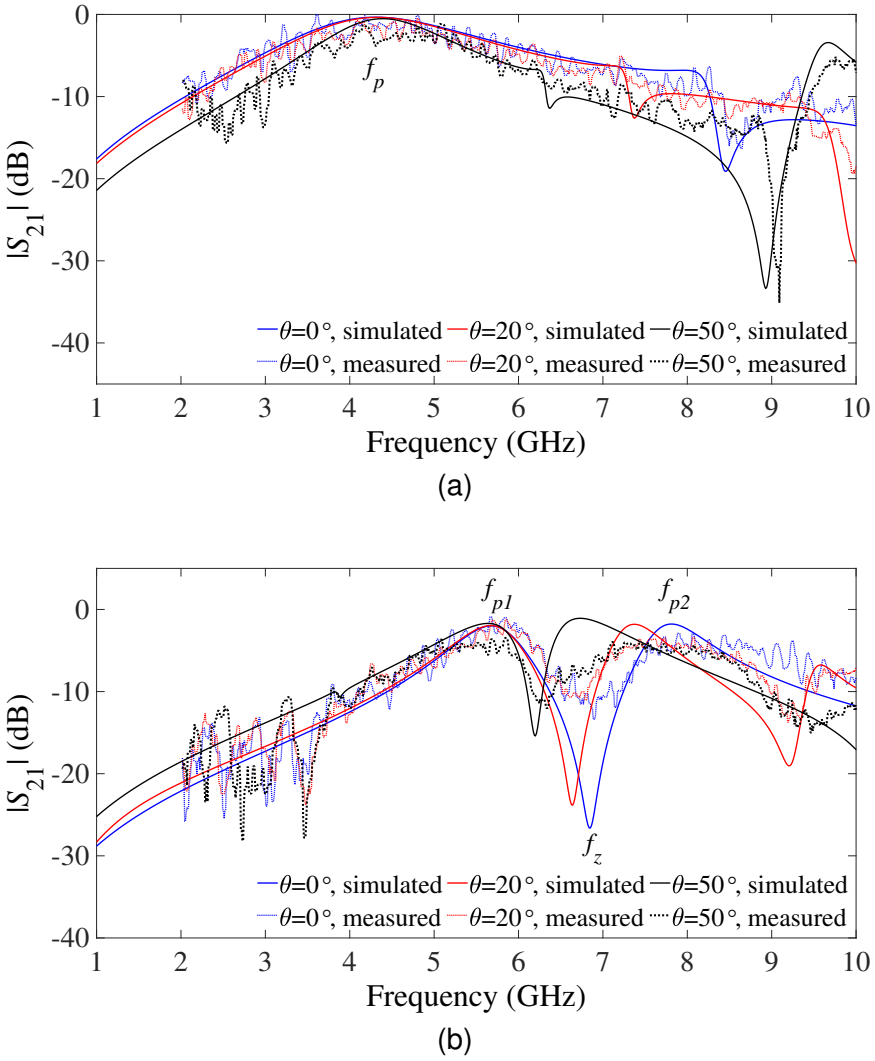


Fig. 13. Simulated and measured results for (a) TE and (b) TM polarization of ideal RCFSS in the off-state.

Brazilian Microwave and Optoelectronics Society-SBMO
Brazilian Society of Electromagnetism-SBMag
received 10 Jan 2026; for review 31 Mar 2026; accepted 19 Jun 2026
Editor: Carlos E. Capovilla Associate Editor: Rafael A. Penchel
© 2026 SBMO/SBMag
ISSN 2179-1074

B. RCFSS Results

The passive CFSSs provided an understanding of the response that the proposed structure can offer. The next step in the design was to insert the PIN diodes to characterize the real response. Different levels of voltage were applied across the shunt diodes, from 0.0 V to 2.0 V with steps of 0.2 V, and the frequency response of the proposed structure was observed. The PIN diodes allow current flows from 0.8 V on. We display the results of three cases when the PIN diodes are biased with 2.0 V (forward region, Fig. 14), 0.6 V (threshold region, Fig. 15) and 0.0 V (reverse region, Fig. 16).

As predicted from the passive CFSS in the on-state, the practical RCFSS presents similar results for both polarizations. When the PIN diodes are forward biased with V = 2.0 V, the elements are coupled and two transmission maxima are observed at f_{p1} = 2.28 GHz and f_{p2} = 6.53 GHz from the simulated results, and f_{p1} = 2.1 GHz and f_{p2} = 6.9 GHz from the measured results for the TE polarization at normal incidence (Fig. 14a). The transmission minimum is found at 3.86 GHz and 3.64 GHz from the numerical and measured results, respectively. The maximum difference between the simulated and measured results for the first transmission maximum, the transmission minimum and the

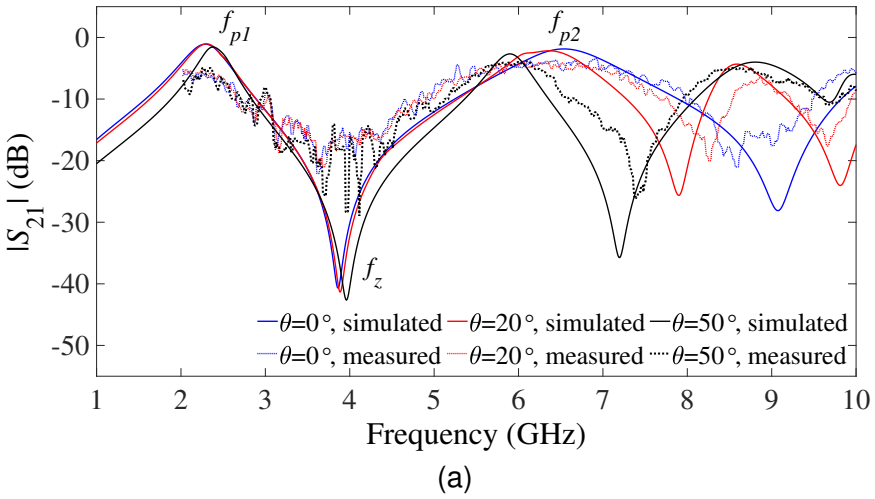


Fig. 14. Simulated and measured results for (a) TE and (b) TM polarization of practical RCFSS in the on-state, biasing diodes with V = 2.0 V.

Brazilian Microwave and Optoelectronics Society-SBMO
Brazilian Society of Electromagnetism-SBMag
received 10 Jan 2026; for review 31 Mar 2026; accepted 19 Jun 2026
Editor: Carlos E. Capovilla Associate Editor: Rafael A. Penchel
© 2026 SBMO/SBMag
CC BY
ISSN 2179-1074

second transmission maximum are 10.96%, 5.69% and 5.66%, respectively. Note that the results agree with the ones predicted by the on-state passive CFSS for all incidence angles, and, again, it is observed that as θ increases, the second transmission maximum reduces while the first transmission maximum and transmission minimum remain the same. Fig. 14b shows the results for the TM polarization, the response is less sensitive to the diode state because the electric field is nearly null at the switching point, as discussed in Section II. Nevertheless, the bias lines perturb the current path and contribute to the higher-frequency transmission features. In this case, two transmission maxima at 5.7 GHz and 7.83 GHz with a transmission minimum at 6.87 GHz are observed numerically. The experimental characterization obtained these resonant frequencies at f_{p1} = 5.92 GHz, f_{p2} = 8.57 GHz and f_z = 6.99 GHz. Again, the results from the on-state RCFSS are observed to follow the ones obtained by the on-state passive CFSS, including the results by varying θ.

The transmission spectra of the proposed structure when the PIN diodes are biased with the threshold voltage, V = 0.6 V, is shown in Fig. 15. In this condition, the equivalent circuit of the PIN diode consists of a capacitor with a shunt resistor. The resistance of this resistor is not low enough to let the current

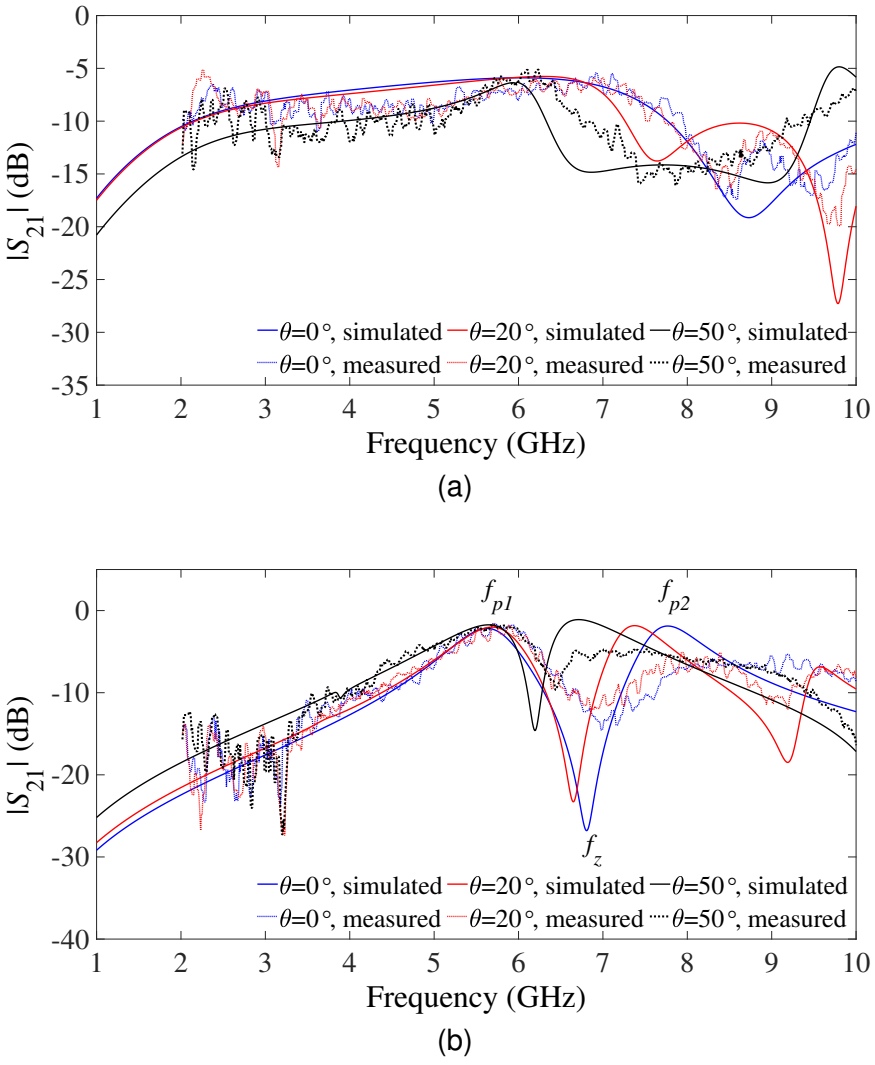


Fig. 15. Simulated and measured results for (a) TE and (b) TM polarization of practical RCFSS with diodes in the threshold region, biased with V = 0.6 V.

Brazilian Microwave and Optoelectronics Society-SBMO
Brazilian Society of Electromagnetism-SBMag
received 10 Jan 2026; for review 31 Mar 2026; accepted 19 Jun 2026
Editor: Carlos E. Capovilla Associate Editor: Rafael A. Penchel
© 2026 SBMO/SBMag
ISSN 2179-1074

flow freely. This resistance results in an attenuation of the passband with an average value of -7-dB (simulated) and -8-dB (measured) over the frequency range from 2 GHz to 8 GHz for the TE polarization, as shown in Fig. 15a. This intermediate state is useful because it enables control of the transmitted signal level, which may be applied in 5G and reconfigurable intelligent-surface scenarios to reduce excessive incident power, avoid receiver front-end saturation, mitigate interference, or provide an AGC-like spatial attenuation function. As mentioned above, in the TM polarization the biased PIN diode has no effect on the frequency response of the structure, thus the two transmission maxima with a transmission minimum are seen as illustrated in Fig. 15b. The simulated and measured results agree for both polarizations.

Fig. 16 illustrates the transmission spectra of the RCFSS when the PIN diodes are reverse biased, V = 0.0 V, disconnecting the upper and lower patch arms, which show to have similar response to the ones for the off-state passive CFSS. For the TE polarization, one transmission maximum is observed at 3.89 GHz (simulated) and 3.75 GHz (measured) at $\theta = 0°$ (Fig. 16a) with maximum difference of 3.6%. The structure shows to be stable at different angles of incidence with maximum resonant

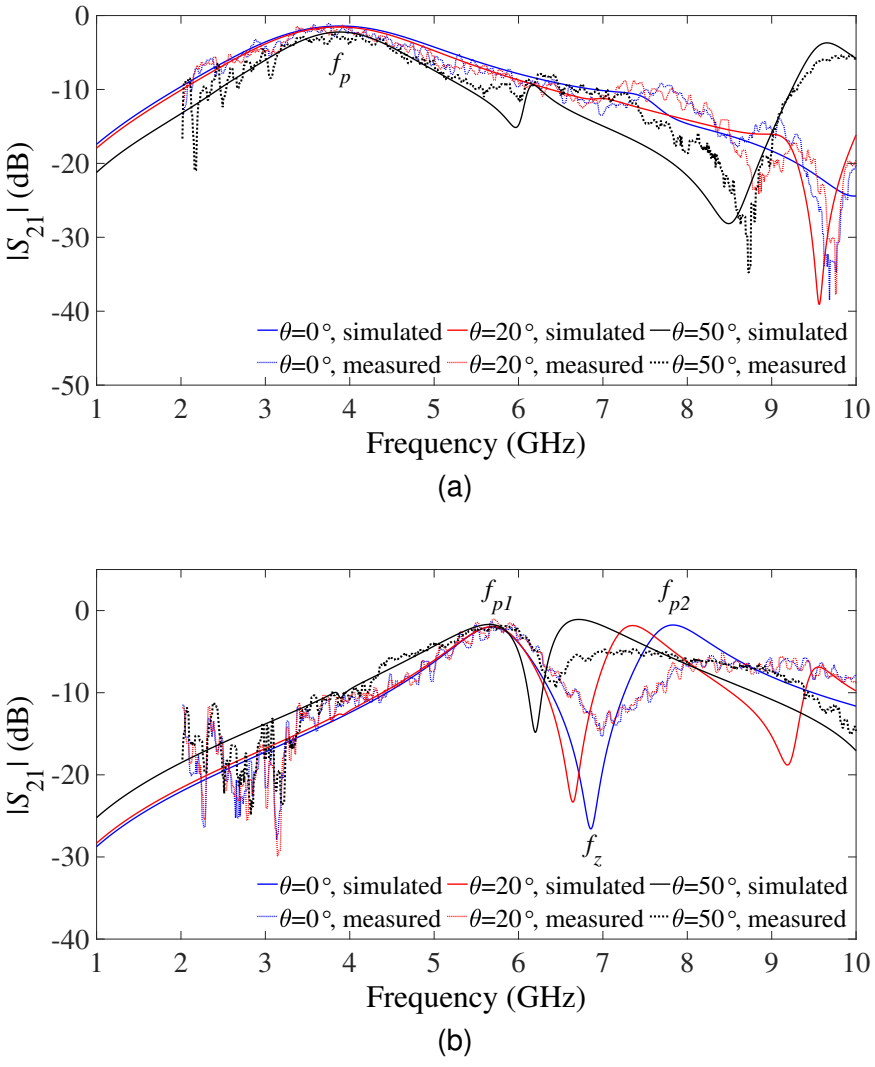


Fig. 16. Simulated and measured results for (a) TE and (b) TM polarization of practical RCFSS in the off-state, biasing diodes with V = 0.0 V.

Brazilian Microwave and Optoelectronics Society-SBMO
Brazilian Society of Electromagnetism-SBMag
received 10 Jan 2026; for review 31 Mar 2026; accepted 19 Jun 2026
Editor: Carlos E. Capovilla Associate Editor: Rafael A. Penchel
© 2026 SBMO/SBMag
ISSN 2179-1074

frequency deviation of 0.26% and 5.33% for the numerical and experimental results, respectively, from $\theta = 0^\circ$ to 50°. The reverse-biased state is particularly important because it demonstrates that the same frequency region that behaves as a stopband in the forward-biased state can be switched to a passband when the diodes are reverse biased. Therefore, the proposed RCFSS can switch between transmission and rejection by changing the diode bias. Fig. 16b shows the simulated and measured transmission coefficient in the TM polarization, which present the same response as the ones from the previous biasing conditions.

Overall, the practical RCFSS demonstrates three distinct electromagnetic states using only one PIN diode per unit cell. In the forward-biased state, it provides a dual-passband response with an intermediate stopband. In the reverse-biased state, it provides a single-passband response. In the threshold-voltage state, it provides an attenuated-transmission response. These operating modes provide flexible control of transmission, rejection, and signal attenuation, which is attractive for adaptive filtering and transmission-control functions in 5G-oriented reconfigurable surfaces.

C. Performance Assessment

The elements of the proposed RCFSS were designed based on the duality theorem. The results presented in Sections IV-A and IV-B confirm that a single PIN diode per unit cell can reconfigure the structure's frequency response, achieving a switchable reflection and transmission with a -10-dB bandwidth of approximately 2.3 GHz. At the off-state resonant frequency, the structure achieves isolations of -40.7 dB (simulated) and -22 dB (measured) between on and off states. In the on-state for the passive and active structures, a dual-passband response is obtained. Switching to the off-state (practical case with PIN diode or ideal case with a gap g) yields a single-passband at 3.75 GHz. Furthermore, biasing the diodes at the threshold voltage produces an attenuated-passband response across the band, with an average transmission coefficient of -8 dB and no distinct transmission maxima or minima.

A comparison of the proposed RCFSS with related works is provided in Table I, evaluating parameters such as configuration type, tuning method, reconfigurable properties, biasing network, operating frequencies and number of bands, unit cell dimensions, angular stability, and additional requirements. Compared to prior designs, the proposed structure advances the state of the art through its simplicity and versatility. For instance, while the design in [18] also supports three operational modes (single-passband, dual-passband, and no-passband), it requires a complex multi-layer setup with three metal layers, two dielectrics, eight PIN diodes per unit cell, and separate bias networks with vias, resulting in higher fabrication complexity and a larger unit cell size ($0.66\lambda \times 0.66\lambda$). In contrast, our design uses only two metal layers on a single dielectric, one PIN diode per unit cell, and a simple parallel-row biasing network without vias or additional lumped elements, enabling three modes—including a unique attenuated-passband mode via the diode's threshold state—while maintaining a compact unit cell ($0.11\lambda \times 0.11\lambda$) and low power consumption (2 V DC).

Similarly, the varactor-tuned design in [27] offers superior miniaturization ($0.05\lambda \times 0.05\lambda$) and angular stability (up to 60°), but it employs 12 varactors per unit cell and two independent DC bias networks with vias and AC-blocks, limiting it to dual-passband tuning without the ability to switch to single- or attenuated-passband modes at fixed frequencies or exploit diode threshold behavior. Our approach, with fewer active components and a streamlined configuration, achieves comparable

Brazilian Microwave and Optoelectronics Society-SBMO received 10 Jan 2026; for review 31 Mar 2026; accepted 19 Jun 2026
Brazilian Society of Electromagnetism-SBMag Editor: Carlos E. Capovilla Associate Editor: Rafael A. Penchel
© 2026 SBMO/SBMag
ISSN 2179-1074

TABLE I. Comparison of proposed reconfigurable FSS with other reported ones.

Ref.	Configura-tion	Tuning method	Reconfig. properties	Biasing network	Freq. (GHz)	No. of bands	Unit cell size	Ang. stab.	Power and other requirements
[16]	3-metal and 2-dielectric	1-PIN-diode loaded	Switchable stop-band frequency	Point-to-point feeding	5.2 and 8.6	Single	$0.31\lambda \times 0.31\lambda$	30°	Requires single-chip microcomputer
[18]	3-metal and 2-dielectric	8-PIN-diodes loaded	Switchable pass/no-pass band	Two bias networks within array and extra ground layer	3.03 and 4.33	Single, dual and none	$0.66\lambda \times 0.66\lambda$	40°	Requires DC power supplies, voltage not reported
[21]	2-metal and 1-dielectric	4-varactors loaded	Tunable pass-band frequency	Bias network within array and extra ground layer with lumped devices	2.94–5.66	Single	$0.12\lambda \times 0.12\lambda$	Not avail-able	Requires 18-V DC voltage
[23]	1-metal and 1-dielectric	Folding	Switchable single to dual stopband	Not designed	2 and 2.8	Single and Dual	$0.67\lambda \times 0.67\lambda$	45°	Require driving apparatus
[26]	1-metal and 1-dielectric	Rotating blinds	Tunable stop-band frequency	Not designed	3.2–5.5	Single	$0.19\lambda \times 0.16\lambda$	60°	Require driving apparatus
[27]	2-metal and 1-dielectric	12-varactors loaded	Independently tunable pass-band frequency	Two bias networks and lumped devices in extra layer	2.28–4.66 and 5.44–11.3	Dual	$0.05\lambda \times 0.05\lambda$	60°	Requires DC power supplies, voltage not reported
This work	2-metal and 1-dielectric	1-PIN-diode loaded	Switchable pass/stop/ attenuated-pass band	Parallel feeding	3.75 or 2.1 and 6.9	Single, dual and none	$0.11\lambda \times 0.11\lambda$	50°	Requires 2-V DC voltage

Brazilian Microwave and Optoelectronics Society-SBMO
Brazilian Society of Electromagnetism-SBMag
received 10 Jan 2026; for review 31 Mar 2026; accepted 19 Jun 2026
Editor: Carlos E. Capovilla Associate Editor: Rafael A. Penchel
© 2026 SBMO/SBMag
CC BY
ISSN 2179-1074

miniaturization relative to the lower operating band while providing broader reconfigurability, including passband/stopband switching at 3.75 GHz.

The proposed RCFSS extends the authors' previous passive coupled-complementary FSS in [38], where fixed dual- and triple-passband responses were achieved using stacked four-arm-star patch/slot elements and offset configurations, and also differs from the reconfigurable V-shaped FSS in [39], which uses a simpler single-metal-layer structure to switch stopband responses and generate a Fano resonance. In contrast, the present design introduces one PIN diode per unit cell and an integrated bias network in a complementary patch-slot configuration, enabling the same surface to switch between dual-passband, single-passband, and attenuated-passband responses. Its main novelty is the exploitation of the PIN-diode threshold region to obtain a controlled attenuation state, in addition to the on/off switching between transmission states.

Overall, these comparisons demonstrate that the proposed RCFSS excels in fabrication ease, compactness, reduced component count, and multi-mode operation. The proposed design is particularly attractive for adaptive filtering and reconfigurable transmission-control applications, where low-complexity implementation, low-voltage operation, and the ability to switch among passband, stopband, and controlled-attenuation responses are required. Although the referenced active FSS designs require external DC biasing, their current and total power consumption are not reported, preventing a direct quantitative comparison.

V. Conclusion

This paper introduces a novel reconfigurable complementary-inspired FSS that achieves single-, dual- and attenuated-passband responses through the use of a single PIN diode per unit cell, leveraging its forward-biased, reverse-biased, and threshold states. The structure features a single dielectric substrate with dual metallizations—one slot-type array and its complementary patch array—integrated with an immersed biasing network designed for parallel-row control without vias or additional layers. Key results demonstrate robust performance: the on-state yields dual passbands with operating frequencies at 2 and 6.9 GHz; the off-state provides a single passband at 3.75 GHz; and the threshold state results in an attenuated passband with an average transmission coefficient of -8 dB across the band. Isolations between on and off states reach -40.7 dB (simulated) and -22 dB (measured) at the off-state resonant frequency.

Compared to existing works, this design advances simplicity and functionality, using fewer active components (one PIN diode versus up to 12 varactors or 8 PIN diodes in prior designs) and a less complex configuration (single substrate without multi-layer biasing or mechanical actuators), while enabling unique mode switching—including passband-to-stopband transitions at the same frequency—for enhanced versatility. These characteristics are practically relevant for 5G applications, such as reconfigurable intelligent surfaces that facilitate adaptive signal control, beam steering in smart antennas, and interference mitigation in dynamic environments by toggling between transmissive and reflective behaviors.

Despite these strengths, limitations include a moderate angular stability (50° versus 60° in some designs) and reliance on PIN diode characteristics, which may introduce minor losses in practical deployments. Future work could explore integration with tunable varactors for continuous frequency adjustment, multi-diode configurations for polarization insensitivity, or hybrid electrical-mechanical approaches to extend angular stability beyond 60°.

Brazilian Microwave and Optoelectronics Society-SBMO received 10 Jan 2026; for review 31 Mar 2026; accepted 19 Jun 2026
Brazilian Society of Electromagnetism-SBMag Editor: Carlos E. Capovilla Associate Editor: Rafael A. Penchel
© 2026 SBMO/SBMag
ISSN 2179-1074

DATA AVAILABILITY STATEMENT

All the data in this manuscript is provided in this publication.

REFERENCES

[1] B. A. Munk, *Frequency selective surfaces: theory and design*. John Wiley & Sons, 2005.

[2] R. S. Anwar, L. Mao, and H. Ning, "Frequency selective surfaces: a review," *Applied Sciences*, vol. 8, no. 9, pp. pp. 1689:1–1689:46, 2018.

[3] Y.-L. Su, C.-C. Jian, Y.-L. Lee, C.-H. Li, and T. Lohrey, "Dichroic sub-reflector for wide band techniques for single offset antenna," *48^{th} European Microwave Conference (EuMC)*, pp. 268–271, 2018.

[4] J. A. Vásquez-Peralvo, J.-M. Fernández-González, P. Valtr, and J. M. Rigelsford, "Inductive frequency selective surface: An application for dichroic sub-reflectors," *IEEE Access*, vol. 8, pp. 22 721–22 732, 2020.

[5] D. F. Mamedes, A. G. Neto, and J. Bornemann, "Reconfigurable corner reflector using pin-diode-switched frequency selective surfaces," *2020 IEEE International Symposium on Antennas and Propagation and North American Radio Science Meeting*, pp. 127–128, 2020.

[6] S. M. Mahmood and T. A. Denidni, "Pattern-reconfigurable antenna using a switchable frequency selective surface with improved bandwidth," *IEEE Antennas and Wireless Propagation Letters*, vol. 15, pp. 1148–1151, 2016.

[7] C. Yang, P. Liu, and X. Zhu, "Circularly polarized microstrip patch antenna array based on fss polarization converter," *2019 International Symposium on Antennas and Propagation (ISAP)*, pp. 1–3, 2019.

[8] D. F. Mamedes, J. Bornemann, and A. G. Neto, "Linear-to-circular polarization converter based on four-arms star fss at 5.2 ghz for 5g applications," *16^{th} European Conference on Antennas and Propagation (EuCAP)*, pp. 1–4, 2022.

[9] S. Habib, G. I. Kiani, and M. F. U. Butt, "Interference mitigation and wlan efficiency in modern buildings using energy saving techniques and fss," *2016 IEEE International Symposium on Antennas and Propagation (APSURSI)*, pp. 965–966, 2016.

[10] M. Gustafsson, A. Karlsson, A. Rebelo, and B. Widenberg, "Design of frequency selective windows for improved indoor outdoor communication," *IEEE Transactions on Antennas and Propagation*, vol. 54, no. 6, pp. 1897–1900, 2006.

[11] M. Pazokian, N. Komjani, and M. Karimipour, "Broadband rcs reduction of microstrip antenna using coding frequency selective surface," *IEEE Antennas and Wireless Propagation Letters*, vol. 17, no. 8, pp. 1382–1385, 2018.

[12] H. B. Baskey and M. J. Akhtar, "Design of flexible hybrid nanocomposite structure based on frequency selective surface for wideband radar cross section reduction," *IEEE Transactions on Microwave Theory and Techniques*, vol. 65, no. 6, pp. 2019–2029, 2017.

[13] Z. Huang, Z. Luo, Y. Zhao, H. Li, K. Si, Y. Han, L. Miao, and J. Jiang, "Tapered resistive sheets and fss absorber loading for the wideband rcs reduction of the elliptic surface at tm polarization," *IEEE Transactions on Antennas and Propagation*, vol. 71, no. 7, pp. 6191–6195, 2023.

[14] D. Xie, X. Liu, H. Guo, X. Yang, C. Liu, and L. Zhu, "A wideband absorber with a multiresonant gridded-square fss for antenna rcs reduction," *IEEE Antennas and Wireless Propagation Letters*, vol. 16, pp. 629–632, 2017.

[15] H. Li, Q. Cao, L. Liu, and Y. Wang, "An improved multifunctional active frequency selective surface," *IEEE Transactions on Antennas and Propagation*, vol. 66, no. 4, pp. 1854–1862, 2018.

[16] H. Yuan, H. Li, X. Fang, Y. Wang, and Q. Cao, "Active frequency selective surface absorber with point-to-point biasing control system," *IEEE Antennas and Wireless Propagation Letters*, vol. 20, no. 8, pp. 1429–1432, 2021.

[17] C. Zhao, C.-F. Wang, and S. Aditya, "Power-dependent frequency-selective surface: Concept, design, and experiment," *IEEE Transactions on Antennas and Propagation*, vol. 67, no. 5, pp. 3215–3220, 2019.

[18] B. Jiang, H. Hu, J. Tian, S. Lei, M. Chen, and B. Chen, "A polarization-insensitive dual-band fss with high selectivity and independently switchable characteristics," *IEEE Antennas and Wireless Propagation Letters*, vol. 22, no. 1, pp. 14–18, 2023.

[19] M. Guo, Y. Zheng, Q. Chen, L. Ding, D. Sang, F. Yuan, T. Guo, and Y. Fu, "Analysis and design of a high-transmittance performance for varactor-tunable frequency-selective surface," *IEEE Transactions on Antennas and Propagation*, vol. 69, no. 8, pp. 4623–4632, 2021.

[20] S. Ghosh and K. V. Srivastava, "Broadband polarization-insensitive tunable frequency selective surface for wideband shielding," *IEEE Transactions on Electromagnetic Compatibility*, vol. 60, no. 1, pp. 166–172, 2018.

[21] Q. Guo, Z. Li, J. Su, J. Song, and L. Y. Yang, "Active frequency selective surface with wide reconfigurable passband," *IEEE Access*, vol. 7, pp. 38 348–38 355, 2019.

[22] S. N. Azemi, K. Ghorbani, and W. S. T. Rowe, "A reconfigurable fss using a spring resonator element," *IEEE Antennas and Wireless Propagation Letters*, vol. 12, pp. 781–784, 2013.

Brazilian Microwave and Optoelectronics Society-SBMO *received 10 Jan 2026; for review 31 Mar 2026; accepted 19 Jun 2026*
Brazilian Society of Electromagnetism-SBMag *Editor: Carlos E. Capovilla Associate Editor: Rafael A. Penchel*
© 2026 SBMO/SBMag CC BY
ISSN 2179-1074

[23] A. Biswas, C. L. Zekios, and S. V. Georgakopoulos, "Transforming single-band static fss to dual-band dynamic fss using origami," *Scientific Reports*, vol. 10, no. 1, pp. pp. 13 884:1–13 884:12, 2020.

[24] S. A. Nauroze, L. Novelino, M. M. Tentzeris, and G. H. Paulino, "Inkjet-printed "4d" tunable spatial filters using on-demand foldable surfaces," *IEEE MTT-S International Microwave Symposium (IMS)*, pp. 1575–1578, 2017.

[25] D. Ferreira, I. Cuiñas, R. F. S. Caldeirinha, and T. R. Fernandes, "3-d mechanically tunable square slot fss," *IEEE Transactions on Antennas and Propagation*, vol. 65, no. 1, pp. 242–250, 2017.

[26] S. A. B, E. F. Sundarsingh, and V. S. Ramalingam, "Mechanically reconfigurable frequency selective surface for rf shielding in indoor wireless environment," *IEEE Transactions on Electromagnetic Compatibility*, vol. 62, no. 6, pp. 2643–2646, 2020.

[27] Y. Rahmani-Shams, S. Mohammd-Ali-Nezhad, A. Nooraei Yeganeh, and S. H. Sedighy, "Dual band, low profile and compact tunable frequency selective surface with wide tuning range," *Journal of Applied Physics*, vol. 123, no. 23, pp. pp. 235 301:1–235 301:6, 2018.

[28] F. Costa, A. Monorchio, and G. Manara, "Efficient analysis of frequency-selective surfaces by a simple equivalent-circuit model," *IEEE Antennas and Propagation Magazine*, vol. 54, no. 4, pp. 35–48, 2012.

[29] J. R. Reis, R. F. S. Caldeirinha, A. Hammoudeh, and N. Copner, "Electronically reconfigurable fss-inspired transmitarray for 2-d beamsteering," *IEEE Transactions on Antennas and Propagation*, vol. 65, no. 9, pp. 4880–4885, 2017.

[30] S. C. Bakshi, D. Mitra, and F. L. Teixeira, "Wide-angle broadband rasorber for switchable and conformal application," *IEEE Transactions on Microwave Theory and Techniques*, vol. 69, no. 2, pp. 1205–1216, 2021.

[31] P. Kong, X.-W. Yu, M. Zhao, Y. He, L. Miao, and J. Jiang, "Switchable frequency selective surfaces absorber/reflector for wideband applications," *Journal of Electromagnetic Waves and Applications*, vol. 29, no. 11, pp. 1473–1485, 2015.

[32] C. Gu, B. S. Izquierdo, S. Gao, J. C. Batchelor, E. A. Parker, F. Qin, G. Wei, J. Li, and J. Xu, "Dual-band electronically beam-switched antenna using slot active frequency selective surface," *IEEE Transactions on Antennas and Propagation*, vol. 65, no. 3, pp. 1393–1398, 2017.

[33] Skyworks Solutions, Inc., *SMP1340 Series: Fast Switching-Speed, Low-Capacitance, Plastic-Packaged PIN Diodes* , 2026. [Online]. Available: https://www.skyworksinc.com/-/media/938AA8A86545442389DADFFBEE0E2741.pdf

[34] J. Babinet, "Mémoires d'optique météorologique. ii. sur les couronnes," *Comptes Rendus Hebdomadaires des Séances de l'Académie des Sciences*, vol. 4, pp. 642–645, 1837.

[35] H. Wang, M. Yan, S. Qu, L. Zheng, and J. Wang, "Design of a self-complementary frequency selective surface with multi-band polarization separation characteristic," *IEEE Access*, vol. 7, pp. 36 788–36 799, 2019.

[36] H. G. Booker, "Slot aerials and their relation to complementary wire aerials babinet's principle)," *Journal of the Institution of Electrical Engineers-Part IIIA: Radiolocation*, vol. 93, no. 4, pp. 620–626, 1946.

[37] E. Jordan and K. Balmain, *Electromagnetic Waves and Radiating Systems*. Prentice Hall, Englewood Cliffs, New Jersey, 1968.

[38] D. F. Mamedes, J. Bornemann, A. G. Neto, and S. L. M. S. Filho, "Dual- and triple-passband coupled-complementary FSSs based on the four-arms star geometry," *IET Microwaves, Antennas & Propagation*, vol. 18, pp. 516–528, 2024.

[39] T. R. d. Sousa, D. F. Mamedes, J. d. S. Souza, and V. P. d. Silva, "Single-and Multi-Stopband Reconfigurable FSS," *Journal of Microwaves, Optoelectronics and Electromagnetic Applications*, vol. 23, no. 04, pp. pp. e2 024 287 661:1–e2 024 287 661:10, 2024.

Brazilian Microwave and Optoelectronics Society-SBMO *received 10 Jan 2026; for review 31 Mar 2026; accepted 19 Jun 2026*
Brazilian Society of Electromagnetism-SBMag *Editor: Carlos E. Capovilla Associate Editor: Rafael A. Penchel*
© 2026 SBMO/SBMag
ISSN 2179-1074